ACS Energy LETTERS

http://pubs.acs.org/journal/aelccp

Transient Voltammetry with Ultramicroelectrodes Reveals the Electron Transfer Kinetics of Lithium Metal Anodes

David T. Boyle, Xian Kong, Allen Pei, Paul E. Rudnicki, Feifei Shi, William Huang, Zhenan Bao, Jian Qin,* and Yi Cui*

Cite This: *ACS Energy Lett.* 2020, 5, 701−709

Read Online

ACCESS | Metrics & More | Article Recommendations | Supporting Information

ABSTRACT: **Fully understanding the mechanism of lithium metal deposition is critical for the development of rechargeable lithium battery anodes. The heterogeneous electron transfer kinetics are an important aspect of lithium electrodeposition, but they have been difficult to measure and understand. Here, we use transient voltammetry with ultramicroelectrodes to explicitly investigate the electron transfer kinetics of lithium electrodeposition. The results deviate from the Butler−Volmer model of electrode kinetics; instead, a Marcus model accurately describes the electron transfer. Measuring the kinetics in a series of electrolytes shows the mechanism of lithium deposition under electron transfer control is consistent with the general framework of Marcus theory. Comparison of the transient voltammetry results to electrochemical impedance spectra provides a strategy for understanding how the interplay of the electron transfer and mass transport resistances affect the morphology of lithium.**

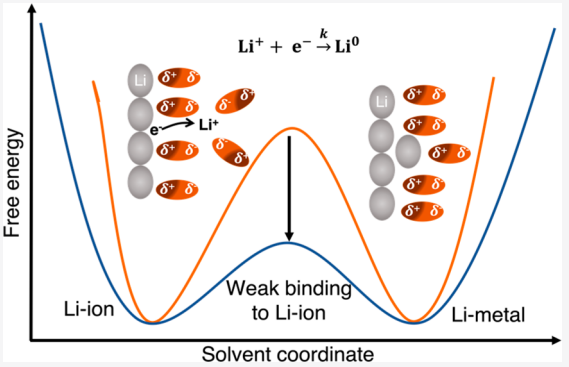

Contemporary portable electronics and electric vehicles continue to increase demand for high energy density lithium batteries.[1] Replacement of graphitic anodes with metallic lithium anodes would improve the energy density of Li-ion batteries, but lithium anodes face many challenges.[2] For lithium metal to become a practical rechargeable battery anode, several processes must be understood and controlled. These processes include the formation of a passivation film called the solid electrolyte interphase (SEI),[3,4] mass transport through the SEI,[5−7] nucleation of lithium on current collectors,[8−10] and interfacial electron transfer. Decades of research have focused on how processes involving the SEI impact the rechargeability of lithium;[11] however, few studies have investigated the $Li^+ + e^- \xrightarrow{k} Li$ electron transfer kinetics,[12,13] which are predicted to influence the morphology of electrodeposited metal.[9,14−23]

Understanding the electron transfer kinetics has historically been challenging, because measurements are typically convoluted by Li-ion transport through the SEI. Earlier studies showed that fast scan cyclic voltammetry (CV) minimizes the effects of SEI, but insufficiently fast scan rates placed the measurements under Nernstian—or mass transport—control, as opposed to kinetic—or electron transfer—control.[20,21,24−28] These studies led to two common assumptions in lithium electrochemistry: (1) the electron transfer is described well by the Butler−Volmer model of electrode kinetics, and (2) the electron transfer resistance is negligible in electrochemical impedance spectra.[29] However, the Nernstian conditions of previous measurements merit a reevaluation of the electron transfer kinetics and these common assumptions.

In this study, we use transient CV with ultramicroelectrodes to explicitly measure the kinetics of the $Li^+ + e^- \xrightarrow{k} Li$ electron transfer reaction with fresh lithium surfaces. We discover that the kinetics deviate from the commonly assumed Butler−Volmer model and are accurately described by Marcus models of electrode kinetics. By exploring the electron transfer kinetics in a series of electrolytes, we find that the kinetics are indeed consistent with the general framework of Marcus theory. This finding opens a strategy for understanding how the interplay of electron transfer and mass transport influence the morphology of electrodeposited lithium via comparison of the transient CV results and electrochemical impedance

Received: January 6, 2020
Accepted: February 3, 2020
Published: February 3, 2020

https://dx.doi.org/10.1021/acsenergylett.0c00031
ACS Energy Lett. 2020, 5, 701−709

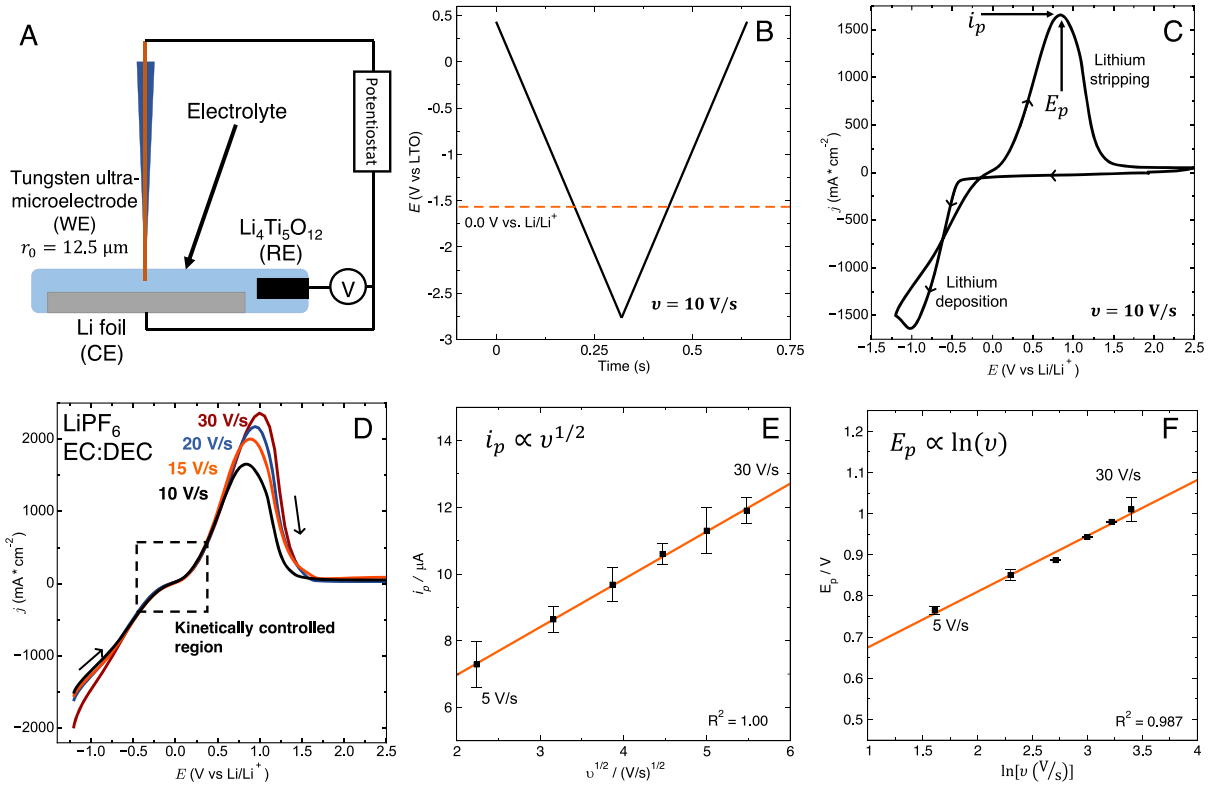

Figure 1. Ultramicroelectrodes can measure the electron transfer kinetics of lithium metal deposition and dissolution. (A) Schematic of the ultramicroelectrode cell. (B) A representative potential profile shows that the experiment is completed in less than one second. (C) A representative full voltammogram for the transient CV in 1 M $LiPF_6$ in EC:DEC. (D) The reverse sweep of the CV experiment with 1 M $LiPF_6$ in EC:DEC shows that there is a kinetically controlled region close to the formal potential of lithium. Forward sweeps are removed for clarity. (E) The i_p varies linearly with $\upsilon^{1/2}$, and (F) E_p varies linearly with $\ln(\upsilon)$, which indicates that the CV experiment is fully irreversible—or under kinetic control near the formal potential. Error bars represent the standard deviation of at least three experiments at each scan rate.

spectroscopy (EIS). Overall, the mechanism of lithium electrodeposition developed herein can guide the engineering of functional electrolytes and interphases for lithium anodes.

A transient experiment is required to accurately measure the $Li^+ + e^- \xrightarrow{k} Li$ electron transfer kinetics. Ultramicroelectrodes have a small cell time constant, so transient CV measurements can be made without distortion of the voltammogram.[30] Figure 1A shows a schematic of the electrochemical cell with a tungsten ultramicroelectrode (r_0 = 12.5 μm), lithium counter electrode, and $Li_4Ti_5O_{12}$ (LTO) reference electrode. Figure 1B shows the potential profile of the experiment with a transient scan rate (υ) of υ = 10 V/s, and Figure 1C shows a representative iR_u-corrected voltammogram with 1 M $LiPF_6$ in 1:1 v:v ethylene carbonate: diethyl carbonate (EC:DEC), where the cathodic current is negative (details of iR_u compensation are presented in Methods and Figure S21 in the Supporting Information). The scan starts at about 2.5 V versus Li/Li^+ and scans negatively to −1.2 V. Once the nucleation overpotential is overcome, lithium deposits on the ultramicroelectrode, and the curve displays a characteristic nucleation loop for metal deposition onto a substrate.[31] When the potential reaches −1.2 V vs Li/Li^+, the direction of the scan is reversed to measure the kinetics.

The transient scan rate serves two purposes: (1) it minimizes the influence of an SEI on the measurement;[20] (2) it places the experiment under kinetic (electron transfer) control at the lithium electrolyte interface, not mass transport control through the electrolyte or an SEI. Because the time scale of the measurement (<1 s) is shorter than the time scale of passivation by an SEI[32] (Figure 1B), convoluting effects of SEI are minimized[20] (Methods and Figure S1 in the Supporting Information). Varying υ shows whether the measurement is under kinetic control. If υ is too slow, then $i \propto \upsilon^{1/2}$ at all points, which indicates the experiment is Nernstian, or mass transport controlled.[30] If the measurement is under kinetic control, then the peak current (i_p) scales linearly with $\upsilon^{1/2}$, the peak potential (E_p) scales linearly with the logarithm of υ, and the current is independent of υ near the equilibrium potential (E_{eq}).[30] Panels D–F of Figure 1 show the effect of υ on the forward sweep of the voltammogram. The scaling of $i_p \propto \upsilon^{1/2}$ and $E_p \propto \ln(\upsilon)$ for υ > 5 V/s (Figures 1E,F and S3) verifies that these measurements are controlled by electron transfer. Additionally, the current is independent of υ near E_{eq} (Figure 1D), further confirming that the measurement is under kinetic control and is not convoluted by effects from an SEI (Figure S1). All data reported below use $\upsilon \geq$ 10 V/s, because the requisite υ depends on the heterogeneous rate constant of each electrolyte (details are provided in Methods in the Supporting Information).

The standard rate constant of the $Li^+ + e^- \xrightarrow{k} Li$ electron transfer reaction can be calculated via a linear relationship between $\ln(i_p)$ and E_p, but the method assumes that the Butler–Volmer model of electrode kinetics is valid (Figures S2 and S3).[30,33] Alternatively, Reinmuth[34] and Nicholson et al.[35] showed that the region near E_{eq} where the current is <10% of

https://dx.doi.org/10.1021/acsenergylett.0c00031
ACS Energy Lett. 2020, 5, 701−709

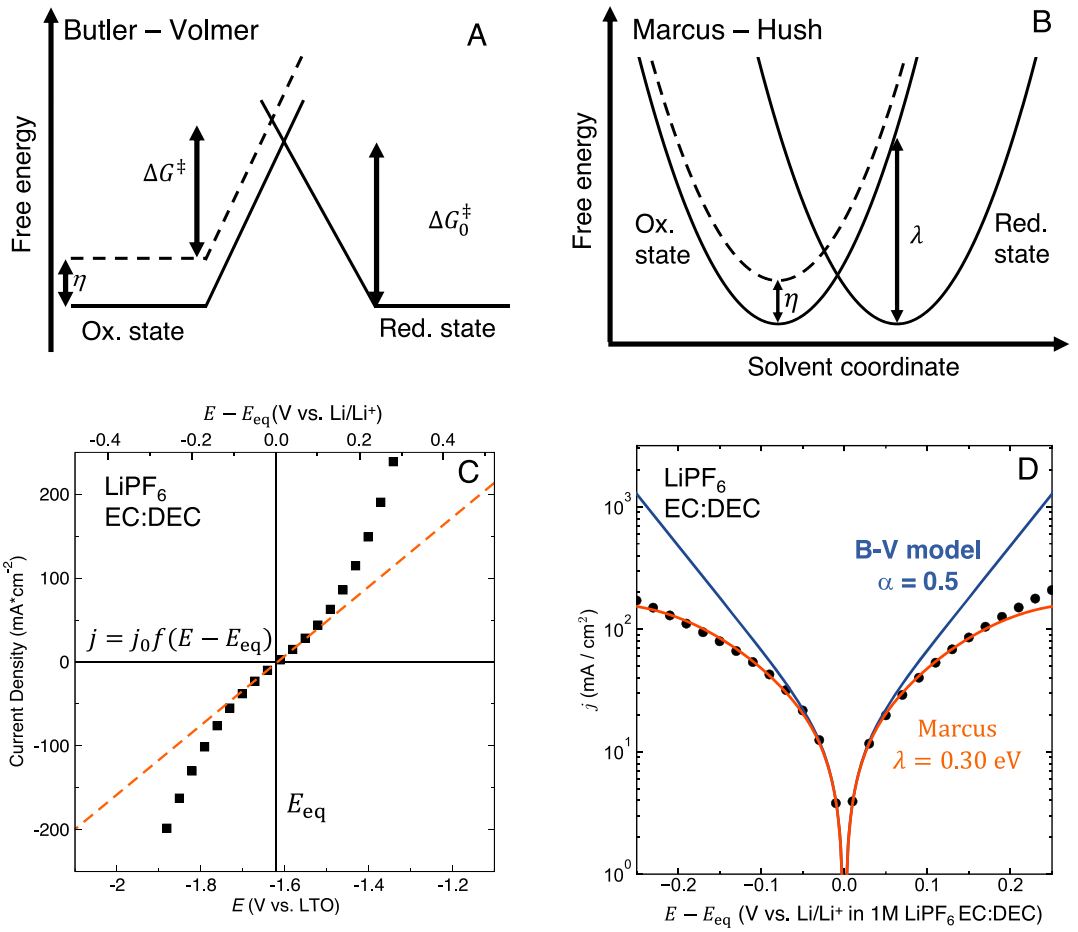

Figure 2. Marcus models of charge transfer accurately describe the electron transfer kinetics of the Li/Li$^+$ redox couple, while the Butler−Volmer model fails when $E - E_{eq} > |\pm 50$ mV|. (A) Schematic of the potential energy surface in the Butler−Volmer model. (B) Schematic of the potential energy surface in the Marcus−Hush model. (C) Representative CV data from the box labeled "kinetically controlled region" in Figure 1D. Only the data <10% of i_p is included. The dashed orange line is the linear least-squares fit to $j = j_0 f(E - E_{eq})$. (D) Comparison of the Butler−Volmer and Marcus−Hush model for 1 M $LiPF_6$ in EC:DEC. CV data are the black dots; Butler−Volmer is the solid blue line, and Marcus−Hush is the solid orange line.

i_p, labeled the kinetically controlled region in Figure 1D, can be directly fit to kinetic models with negligible error. This method can conveniently test whether the Butler−Volmer model is valid for the electrodeposition of lithium metal.

The commonly assumed Butler−Volmer model is the electrochemical equivalent to the Arrhenius model of chemical kinetics. Figure 2A shows a schematic of the potential energy surface, where the intersection of two planes from the initial to final state is the transition state. When mass transfer effects are negligible, the model predicts a current density−potential (j−E) relationship of $j = j_0[e^{(1-\alpha)f(E-E_{eq})} - e^{-\alpha f(E-E_{eq})}]$, where j_0 is the exchange current density, f the inverted thermal voltage $\left(\frac{F}{RT}\right)$, E the potential, and α the transfer coefficient. The transfer coefficient describes the strength of the dependence of the rate on potential and is assumed to be constant. Panels C and D of Figure 2 show that the Butler−Volmer model captures only the data at low overpotentials where the model collapses to the linear form of $j = j_0 f(E - E_{eq})$. Averaging the low overpotential slope of several experiments for $LiPF_6$ in EC:DEC gives $j_0 = 10.4 \pm$ mA/cm^2 (Figure 2C). This value of j_0 is 2 orders of magnitude greater than that from EIS measurements (Figure S4). The larger j_0 is further evidence that an SEI does not convolute the measurement,[20] as EIS spectra include impedance from the transport of Li ions through an SEI.[29] At higher overpotentials of $E - E_{eq} > |\pm 50$ mV|, the data deviates from the symmetric Butler−Volmer model, and a curved Tafel plot is observed (Figure 2D). Figure S5 shows that arbitrary fitting of the data to the Butler−Volmer model gives unreliable and unphysical values of α and j_0, so an alternative description of electrode kinetics is required.

Marcus-based theories of electrode kinetics describe the potential energy surface as two parabolas that represent the collective coordinate of the solvent in the initial and final states (Figure 2B).[36−38] The curvature of the potential energy surface does not change the functional form of current density, $j = j_0[e^{(1-\alpha)f(E-E_{eq})} - e^{-\alpha f(E-E_{eq})}]$, but makes α potential-dependent, i.e. $\alpha = \frac{1}{2} + \frac{e(E - E_{eq})}{4\lambda}$, where λ is the reorganization energy and e is the charge of an electron.[39] The key parameter, λ, corresponds to the energy required to reorganize the solvent in response to different distributions of charge in the initial and final states. Marcus models of charge transfer have been successfully applied to the analysis of electrode kinetics;[38] the Marcus−Hush model used here is the low overpotential approximation of the Marcus−Hush−Chidsey (MHC) formal-

https://dx.doi.org/10.1021/acsenergylett.0c00031
ACS Energy Lett. 2020, 5, 701−709

Table 1. Summary of UME Data and Contribution of $R_{c.t.}$ to EIS Spectra[a]

electrolyte	j_0 (mA/cm^2)	Λ (eV)	$R_{c.t.}^{UME}$ (Ω·cm^2)	$R_{int.}^{EIS}$ (Ω·cm^2)	$R_{c.t.}^{UME}/R_{int.}^{EIS}$ %
$LiAsF_6$ (EC:DEC)	42.3 ± 4.3		0.56 ± 0.06	449 ± 23	0.12% ± 0.02%
$LiPF_6$ (EC:DEC)	10.4 ± 0.8	0.30 ± 0.02	2.5 ± 0.2	133 ± 6	1.9% ± 0.2%
$LiClO_4$ (EC:DEC)	6.5 ± 1.2	0.32 ± 0.01	3.9 ± 0.7	32.6 ± 0.6	12% ± 2%
LiI (EC:DEC)	4.9 ± 1.6	0.33 ± 0.01	5.7 ± 1.8	22.2 ± 4.2	26% ± 10%
LiTFSI (EC:DEC)	6.5 ± 0.8	0.32 ± 0.01	4.3 ± 0.5	71.9 ± 3.5	6.0% ± 0.8%
LiFSI (EC:DEC)	4.0 ± 1.1	0.34 ± 0.02	5.7 ± 1.6	37.7 ± 8.3	15% ± 5%
LiFSI (DME)	29.8 ± 0.7		0.75 ± 0.02	140 ± 39	0.54% ± 0.15%
$LiPF_6$ (EC:DEC 10% FEC)	16.0 ± 2.0	0.28 ± 0.02	1.6 ± 0.2	165 ± 21	1.0% ± 0.2%
$LiPF_6$ (DEC)	3.7 ± 1.1	0.34 ± 0.01	6.9 ± 2.0	32.8 ± 0.4	21% ± 6%
$LiPF_6$ (PC)	2.6 ± 0.6	0.34 ± 0.01	9.9 ± 2.3	827 ± 175	1.1% ± 0.3%

[a]A graphical summary of the dimensionless Wagner number is included in Figure S15.

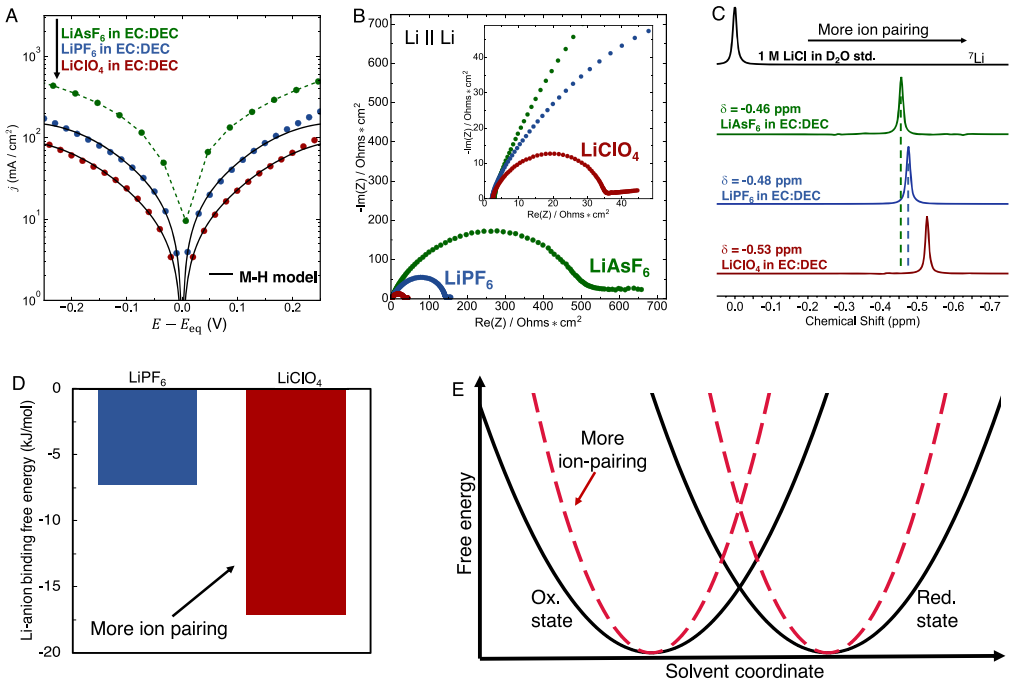

Figure 3. Ionic activity of Li ions dictates the rate of electron transfer in electrolytes with the same solvent. (A) Tafel plots of $LiAsF_6$ (green, υ = 20 V/s), $LiPF_6$ (blue, υ = 10 V/s), and $LiClO_4$ (red, υ = 10 V/s) in EC:DEC. The solid black lines show the corresponding Marcus fits. $LiAsF_6$ is dashed because the experiment is not under total kinetic control. (B) Corresponding Nyquist plots of Li || Li symmetric cells in each electrolyte. (C) ^{7}Li NMR spectra. (D) Comparison of the binding free energies of Li ions and each anion in EC:DEC calculated by molecular dynamics simulations. (E) Schematic of the effect of ion pairing on the potential energy surface.

ism, as it neglects the Fermi distribution of electronic states in the metal. In the limit of large λ (typically $\lambda > 1.0$ eV) and/or small overpotentials (typically $|E - E_{eq}| < 50$ mV), the Marcus and symmetric Butler–Volmer models are indistinguishable.[30] Once the electron transfer kinetics become facile, the free energy of activation ($\Delta G^{\ddagger}$) and λ decrease, so the $\frac{e(E-E_{eq})}{4\lambda}$ term in α causes the Marcus model to deviate from Butler–Volmer and predict curved Tafel plots.

Figure 2D shows that the Marcus–Hush model accurately reproduces the data, whereas the Butler–Volmer model fails. The calculated value of j_0 is consistent with the linear fit in Figure 2C, and the calculated λ is 0.30 eV for 1 M $LiPF_6$ in EC:DEC. This value of λ, although reasonable, may deviate from the true value, because the effects of the Fermi distribution of electrons in lithium[38,40] and the electrical double layer[30] are neglected. We note that the strong agreement between the data and Marcus–Hush model, and the fact that most of the fitted data is well below the value of λ (i.e., 0.3 eV for $LiPF_6$ in EC:DEC), suggests that neglecting the Fermi distribution does not cause large errors in the calculated λ (details are provided in Methods in the Supporting Information). Furthermore, while application of the full MHC integral may give slightly more accurate predictions of λ, this comes at the cost of additional complexity, which could make implementation of Marcus kinetics into battery models more challenging.

The agreement between the data and the Marcus model is consistent with the predictions of Cogswell,[19] Fawcett,[41] and Pinto et al.[42] that metal deposition has a potential-dependent α. Fawcett proposed a model for ion transfer or desolvation of Li ions through a double layer during lithium amalgamation that uses two asymmetric parabolas as the potential energy surface.[41] The dependence of the rate on potential is similar to

https://dx.doi.org/10.1021/acsenergylett.0c00031
ACS Energy Lett. 2020, 5, 701–709

the Marcus−Hush model, but the Tafel plot would be asymmetric.[41] The symmetry of the data suggests that the electron transfer is rate-limiting in our measurements, not ion transport through the double layer or an SEI. Although desolvation of Li ions from the bulk electrolyte into an SEI can be rate-controlling during normal battery operation,[43] this process can also be ruled out, as desolvation energies are generally larger than the calculated λ values in this work (about 0.5 eV[43] versus 0.30 eV, respectively). A Tafel plot controlled by desolvation into an SEI would not cause the observed curvature of the Tafel plot. Recent theoretical work also showed that Ag^+, Li^+, and Cu^+ approach metal surfaces without loss of solvation energy,[42] further supporting the conclusion that electron transfer is the rate-controlling process.

Because the experiment is controlled by electron transfer, we can propose a mechanism for lithium deposition onto itself under electron transfer control. Marcus theory was originally formulated for outer sphere electron transfer reactions, which would be equivalent to the reduction of a solvated Li ion in the outer Helmholtz plane of the double layer. This type of electron transfer is unlikely here, as the formation of an isolated lithium atom in the double layer would be energetically unfavorable.[42,44] Instead, we propose a mechanism similar to that of Gileadi[44] and Pinto et al.,[42] where ion transfer is also considered. The reaction site is at the inner Helmholtz plane, and the electron transfer to a Li ion is coupled to ion transfer from the reaction site to the metal surface. The parameter λ corresponds to the energy required to reorganize the solvent in response to the different distributions of charge in the Li-ion state and Li-metal adatom state (Figures 2B and S6). The small value of λ is likely caused by the close proximity of the Li ion within the inner Helmholtz plane to the lithium electrode.[42,45] Several electrolytes will be examined below to further test the proposed mechanism.

The observation of Marcus kinetics could have practical implications for lithium batteries. Although curved Tafel plots have been reported for several electrode reactions in batteries,[40,46] almost all models of battery systems assume the Butler−Volmer model is valid.[47] Our data shows that the Butler−Volmer model cannot accurately describe the electrodeposition of lithium. The difference between the Marcus and Butler−Volmer models could cause errors in the predicted behavior of lithium batteries, especially during high-rate charging and discharging. This deviation may also explain varying reports of α and j_0.[14,26,48] Marcus-based kinetics could improve the predictive capabilities of battery models when facile electron transfer processes are present. Values of λ, which would be needed to apply the Marcus theory in battery models,[47] are measured and reported below for many electrolytes (Table 1).

To test the proposed mechanism, we compare the kinetics of a series of salts (Figure 3A) including $LiAsF_6$(green), $LiPF_6$ (blue), $LiClO_4$ (red), each dissolved in EC:DEC. These electrolytes serve as a model system to test the mechanism, as the anions are highly symmetric, and the coordination number of solvent to Li ions, dielectric constant, and viscosity are similar. The Tafel plots for $LiClO_4$, and $LiPF_6$ are well described by the Marcus−Hush model, shown as the black lines in Figure 3A. The $LiAsF_6$ data is not fit to the Marcus−Hush model, because the scan rate is likely too slow for total kinetic control. However, a comparison of the limiting current density j_0 is still reasonable. The apparent j_0 increases in the order $LiClO_4$ < $LiPF_6$ < $LiAsF_6$, and the value of λ expectedly follows the opposite trend, i.e., $LiClO_4$ > $LiPF_6$ (Figure 3A and Table 1), suggesting that the rate of electron transfer is higher with larger anions. LiI in EC:DEC electrolyte further slows the kinetics of electron transfer (Figure S8), though the electrolyte is chemically unstable.[49] To further confirm that the transient CV is controlled by electron transfer, we compare the trend in j_0 to EIS spectra of Li || Li symmetric cells, which are primarily controlled by ion transport through the SEI.[29] The interfacial resistance of Li from EIS measurements (Figure 3B) opposes the trend of j_0 from transient CV and verifies that the transient CV is controlled by electron transfer, not ion transport through an SEI (Figure S7). Electrolytes with bis(fluorosulfonyl)imide (FSI^-) and bis(trifluoromethanesulfonyl)imide ($TFSI^-$) in EC:DEC follow the same trends as the salts investigated above (Table 1 and Figure S8). The j_0 increases in the order LiFSI < LiTFSI, and the value of λ increases in the order LiFSI > LiTFSI.

An increase of j_0 with increasing anion size is likely related to a decrease in the degree of ion pairing. Ion pairing decreases the activity coefficient of Li ions, lowering the chemical potential through $\mu_{Li^+} = \mu^0_{Li^+} + \ln(\gamma c)$, where μ is the chemical potential, μ^0 the ideal chemical potential, γ the activity coefficient, and c the concentration of Li ions. ^{7}Li nuclear magnetic resonance (NMR) spectroscopy and molecular dynamics simulations of $LiClO_4$, $LiPF_6$, and $LiAsF_6$ in EC:DEC confirm that smaller anions cause more ion pairing (Figures 3C,D and S8), which is consistent with previous reports of the same electrolytes.[50] Chemical shifts in the ^{7}Li NMR spectra reveal the variation in the solvation environment of Li ions.[51,52] Because the ClO_4^-, PF_6^-, and AsF_6^- anions have similar coordination to the Li ion[53] and the solvent is unchanged, their relative chemical shifts indicate the relative distribution of ion pairs and fully dissociated ions. The ^{7}Li signal is near −0.5 ppm and shifts upfield in the order $LiAsF_6$ < $LiPF_6$ < $LiClO_4$ (Figure 3C), which is consistent with previous studies.[52] Shifts upfield suggest more ion pairs are formed,[52] as the anion increases the electron density around the Li ion. Molecular dynamics simulations also show that the anion pairing energy to Li ions increases in the order $LiPF_6$ < $LiClO_4$ (Figures 3D and S9). The stronger anion pairing energy to Li ions increases the relative amount of ion pairs and lowers the relative chemical potential of Li ions (Figure S10).

By assuming that the trend in chemical potential is applicable in the interfacial region, the effect of the specific anion on the kinetics can be explained and is consistent with the proposed mechanism and Marcus theory (Figure S6). Stronger attraction between Li ions and anions steepens the curvature of the solvent coordinate, increasing λ and decreasing j_0 (Figure 3E and Table 1). The substantial weakening of the Coulombic attraction between the Li ion and anion once the Li ion is reduced to a Li metal adatom explains how the specific anion affects λ and j_0. The dependence of j_0 on the chemical potential is consistent with early kinetic measurements of lithium amalgamation[12] and Bazant's prediction of the reorganization energy for charge transfer in concentrated solutions: $\lambda \propto 4k_BT\ln\left(\frac{\gamma_{\ddagger}}{(\gamma_{Li^+})^{1/2}}\right)$, where k_B is the Boltzmann constant, T the temperature, $\gamma_{\ddagger}$ the activity coefficient of the transition state, and γ_{Li^+} the activity coefficient of Li ions.[39] Notably, these results differ from previous reports of j_0 for the same salts in propylene carbonate (PC).[15] This work used slow scan rates (υ = 20 mV/s), which

https://dx.doi.org/10.1021/acsenergylett.0c00031
ACS Energy Lett. 2020, 5, 701−709

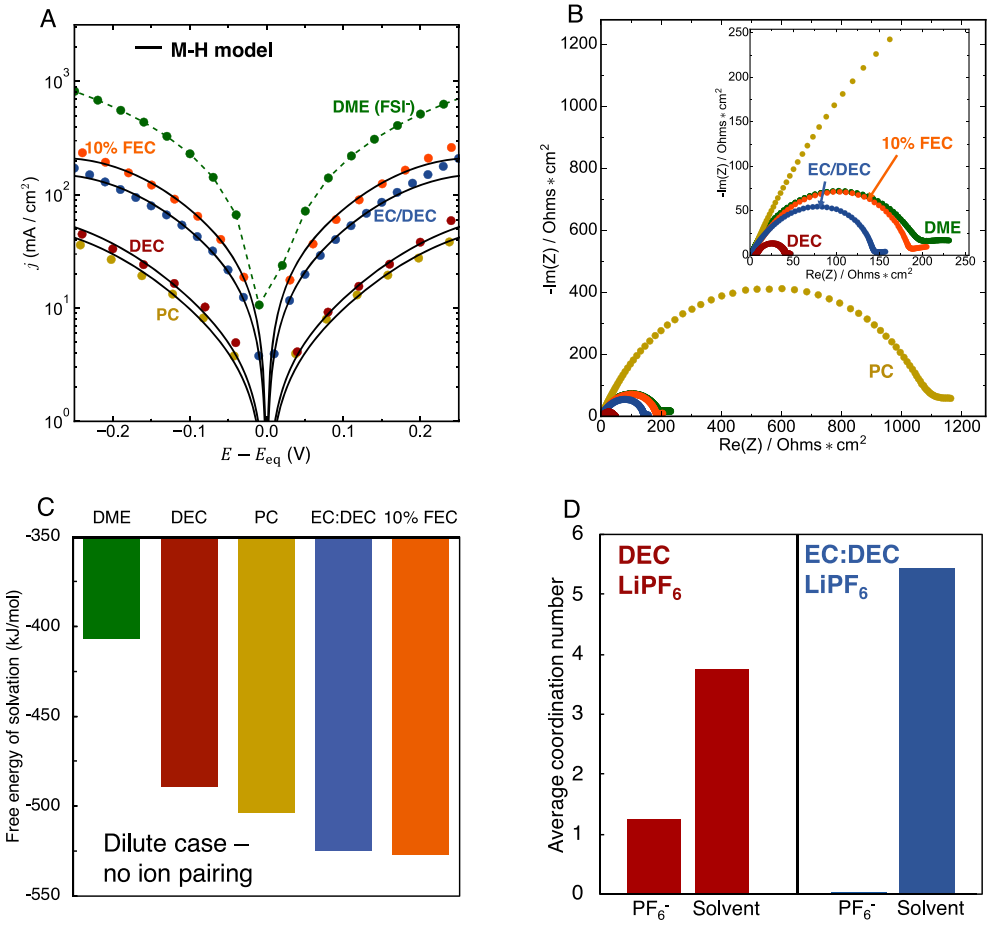

Figure 4. Effect of solvent on the charge transfer kinetics. (A) Tafel plots of $LiPF_6$ in PC (golden, υ = 20 V/s), DEC (red, υ = 20 V/s), EC:DEC (blue, υ = 10 V/s), EC:DEC + 10% FEC (orange, υ = 15 V/s), and DME (green, υ = 50 V/s). (B) Corresponding Nyquist plots of Li || Li symmetric cells. (C) Dilute free energy of solvation for Li ions in each solvent calculated from molecular dynamics simulations. (D) Comparison of the average coordination environment of Li ions in DEC and EC:DEC calculated by molecular dynamics simulations.

cause the measurement to be controlled by mass transport; our experiments explicitly measure the electron transfer kinetics.

To further test the proposed mechanism, we measured the rates of electron transfer with $LiPF_6$ in PC, DEC, EC:DEC, EC:DEC with 10% (by volume) fluoroethylene carbonate (FEC), and LiFSI in dimethoxyethane (DME) (Figure 4A). Each electrolyte is described well by the Marcus model. Similar to the $LiAsF_6$ electrolyte, the scan rate is likely too slow to put the DME experiment under total kinetic control, but a comparison of j_0 can still be made. The j_0 depends on the solvent, which is similar to kinetic measurements of lithium amalgamation,[13] and increases in the order PC < DEC < EC:DEC < EC:DEC + 10%FEC < DME (Figure 4A). The interfacial impedance of Li from EIS increases in the order DEC < EC:DEC < EC:DEC + 10%FEC < DME < PC (Figure 4B), which further verifies that the measurement is not influenced by an SEI, as the j_0 and the total impedance do not correlate directly. Here, ^{7}Li NMR cannot explain the trend in j_0, as different solvents have different solvation structures, dielectric constants, and Guttman donor numbers (Figure S11). We use molecular dynamics simulations to analyze the effect of the solvent.

We first examine the difference between the ether (DME) electrolyte and electrolytes with cyclic carbonates (EC, PC, FEC). Marcus theory and the proposed mechanism predict that λ is small and j_0 is large when the binding strength of the solvent to Li ions is weak. The calculated free energies of solvation of Li ions directly quantify the chemical potential of Li ions in the dilute limit. Figure 4C shows that the free energies of solvation in cyclic carbonates are greater in magnitude than that in DME by 96.41−120.18 kJ/mol. The contribution of ion pairing to the chemical potential of Li ions in 1 M LiFSI/DME does not lower the chemical potential below that of $LiPF_6$ in carbonates (Figure S12). Thus, we attribute the larger j_0 in 1 M LiFSI/DME (29.8 ± 0.7 mA/cm^2) to the weaker interaction between DME and Li ions, which lowers the barrier to electron transfer.

The variation of the free energy of solvation between each carbonate electrolyte is only between 15 and 41 kJ/mol, so the effect of counteranions must also be considered. A switch from $LiPF_6$ in EC:DEC to only DEC decreases the j_0 from 10.4 ± 0.8 mA/cm^2 to 3.7 ± 1.1 mA/cm^2. The molecular dynamics simulations show that the average coordination environment of Li ions in DEC has 1.24 anions and 3.77 solvent molecules within the first solvation shell, whereas EC:DEC has 0.03 anions and 5.44 solvent molecules (Figure 4D). Ion pairing decreases the chemical potential of Li ions in DEC relative to EC:DEC, which consequently increases the barrier to electron transfer. Additionally, individual DEC molecules reside in the first solvation shell for 49.6 ns compared to 5.9 and 30.6 ns for

https://dx.doi.org/10.1021/acsenergylett.0c00031
ACS Energy Lett. 2020, 5, 701−709

EC and DEC, respectively, in EC:DEC electrolyte (Figure S13). The combination of these effects effectively increases λ and lowers j_0 in DEC.

The $LiPF_6$ in PC electrolyte has the lowest j_0, 2.6 ± 0.6 mA/cm^2. Analysis of the free energy of solvation for Li ions in PC initially suggests that j_0 would be larger in PC relative to EC:DEC (Figures 4C and S12); however, this analysis ignores the effect of viscosity on the rate of charge transfer. All the electrolytes considered above have similar viscosities, which allowed us to focus on the effect of the chemical potential. Many studies have reported that the standard rate constant of interfacial electron transfer depends the longitudinal relaxation time of the solvent (τ_L), which is proportional to the viscosity of the solution.[30,54,55] As a result, the standard rate constant can be written as $k_0 = A{\tau_L}^{-\theta}\exp\left(-\frac{\Delta G^{\ddagger}}{RT}\right)$, where A is a prefactor that is independent of τ_L, θ a fraction between 0 and 1, and $\Delta G^{\ddagger}$ the Gibbs free energy of activation.[54] The τ_L is then estimated as $\tau_L \approx 3\frac{V_m}{RT}\left(\frac{\epsilon_o}{\epsilon_s}\right)\eta$, where V_m is the molar volume, $\left(\frac{\epsilon_o}{\epsilon_s}\right)$ the ratio of the optical and static dielectric constants, and η the viscosity.[54] The PC electrolyte has a viscosity of η = 8−10 cP[52] versus η = 3−4 cP[56,57] for 1:1 mixtures of cyclic and linear carbonates. Because 3-fold increases in viscosity can decrease the heterogeneous rate constant by an order of magnitude,[55] the large viscosity of PC explains the lower j_0. This result is consistent with the proposed mechanism and the general framework of Marcus theory, as λ corresponds to reorganization of the solvent.

Cosolvent additives also affect the electron transfer kinetics. Adding 10% (by volume) of the commonly used additive, FEC,[6] to the standard EC:DEC electrolyte increases the j_0 from 10.4 ± 0.8 mA/cm^2 to 16.0 ± 2.0 mA/cm^2 and lowers the solvation free energy by 2.35 kJ/mol (Figure 4A,C). The slightly lower concentration of the 10% FEC solution weakens the interaction between ions (Figure S14), which decreases the extent of ion pairing and increases the j_0 relative to EC:DEC. This result suggests that FEC additives not only result in a more functional SEI[6,7] but also accelerate the electron transfer kinetics.

Overall, the consistency of the kinetics with the general framework of Marcus theory provides insight into how the chemical and physical properties of the electrolyte, or SEI in a practical anode, affect the rate of electron transfer. If the electrolyte, or SEI, binds strongly to Li ions, then the electron transfer kinetics would be slow relative to electrolytes that bind weakly.

In addition to the mechanistic insight provided by transient CV results, a closer comparison of the transient CV and EIS data can estimate the contribution of the electron transfer resistance to the total interfacial impedance of Li anodes. Li || Li EIS measurements contain contributions from both electron transfer and ion-transport through the SEI (Figure 5), but reliable values of the electron transfer resistance were unavailable. Using the transient CV, the measured j_0 of each electrolyte in Table 1 can be converted into an electron transfer resistance via $R_{c.t.}^{UME} = \frac{RT}{Fj_0}$.[30] The total interfacial resistance ($R_{int.}^{EIS}$) can then be calculated from the EIS data by fitting to an equivalent circuit that captures both the electron transfer and ion transport through the SEI[5,7,29,58] (Figures 5 and S18 and Table S1). The first R/C circuit that responds at the highest frequency (ω) corresponds to the electron transfer process, and we find that the electron transfer resistance contributes to 0.12%−26% of the total interfacial resistance measured with EIS (Figure 5). Each contribution is tabulated in Table 1 as $R_{c.t}^{UME}/R_{int.}^{EIS}$. This ratio, a dimensionless Wagner number, is predicted to influence the morphology of lithium deposits.[9,18,19] The transient CV method allows for future investigations of the relationship between the Wagner number and the morphology of lithium via explicit measurement of the electron transfer resistance (Figure S19).

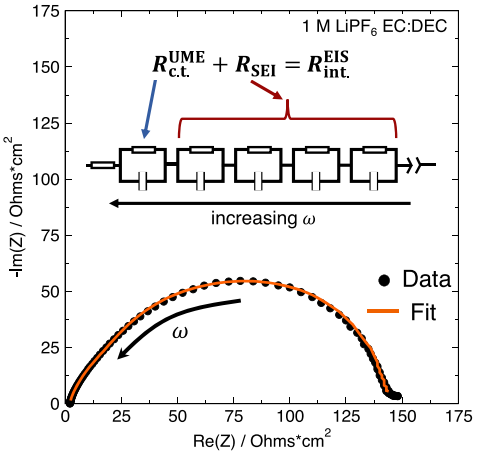

Figure 5. Transient CV can calculate the contribution of the electron transfer resistance to the total impedance of lithium anodes. EIS data of a symmetric Li || Li cell with $LiPF_6$ in EC:DEC electrolyte. The data is fit to an equivalent circuit,[58] shown as an inset, where the first R/C circuit represents the electron transfer (calculated from transient CV), and the second to fifth R/C circuits represent the impedance of the SEI.[5,7,29,58]

Overall, transient CV with ultramicroelectrodes can explicitly measure the $Li^+ + e^- \xrightarrow{k} Li$ electron transfer kinetics with fresh lithium surfaces, providing mechanistic insight into lithium deposition. The kinetics deviate from the Butler−Volmer model; a Marcus-based model accurately describes the kinetics. Varying the electrolyte shows that the electron transfer kinetics are consistent with the general framework of Marcus theory. This consistency provides a molecular picture of the Li/Li^+ electron transfer and shows how the chemical and physical properties of the electrolyte affect the kinetics. In general, the chemical potential of Li ions—or the strength of interaction between the solvent/anions with the Li ion—and the viscosity of the electrolyte control the rate of electron transfer. These results can serve as a basis for testing theoretical models of electron transfer at the lithium/electrolyte interface.[59] Comparison of the transient CV data to EIS data shows the electron transfer resistance contributes to 0.12%−26% of the total interfacial resistance of lithium anodes. These findings provide a specific strategy for understanding how the interplay of electron transfer and mass transfer influences the morphology of electrodeposited lithium. Overall, the elucidation of the mechanism of lithium deposition should accelerate the development of functional electrolytes for lithium batteries.

■ ASSOCIATED CONTENT

Supporting Information

The Supporting Information is available free of charge at https://pubs.acs.org/doi/10.1021/acsenergylett.0c00031.

https://dx.doi.org/10.1021/acsenergylett.0c00031
ACS Energy Lett. 2020, 5, 701−709

Detailed description of the materials and methods, additional transient CV data and traditional analysis, discussion related to the Butler–Volmer model, additional molecular dynamics data, calibration of NMR peaks, schematics for facilitated understanding of the proposed mechanisms, and correlations of the morphology of lithium to the interplay of the electron transfer and mass transport resistances (PDF)

AUTHOR INFORMATION

Corresponding Authors

Jian Qin − *Department of Chemical Engineering, Stanford University, Stanford, California 94305, United States;* orcid.org/0000-0001-6271-068X; Email: jianq@stanford.edu

Yi Cui − *Department of Materials Science and Engineering, Stanford University, Stanford, California 94305, United States; Stanford Institute for Materials and Energy Sciences, SLAC National Accelerator Laboratory, Menlo Park, California 94025, United States;* orcid.org/0000-0002-6103-6352; Email: yicui@stanford.edu

Authors

David T. Boyle − *Department of Chemistry, Stanford University, Stanford, California 94305, United States;* orcid.org/0000-0002-0452-275X

Xian Kong − *Department of Chemical Engineering, Stanford University, Stanford, California 94305, United States;* orcid.org/0000-0001-5602-6347

Allen Pei − *Department of Materials Science and Engineering, Stanford University, Stanford, California 94305, United States;* orcid.org/0000-0001-8930-2125

Paul E. Rudnicki − *Department of Chemical Engineering, Stanford University, Stanford, California 94305, United States;* orcid.org/0000-0003-3518-1721

Feifei Shi − *Department of Materials Science and Engineering, Stanford University, Stanford, California 94305, United States*

William Huang − *Department of Materials Science and Engineering, Stanford University, Stanford, California 94305, United States;* orcid.org/0000-0001-8717-5337

Zhenan Bao − *Department of Chemical Engineering, Stanford University, Stanford, California 94305, United States;* orcid.org/0000-0002-0972-1715

Complete contact information is available at: https://pubs.acs.org/10.1021/acsenergylett.0c00031

Notes

The authors declare no competing financial interest.

ACKNOWLEDGMENTS

Y.C. and J.Q. acknowledge the support from the Assistant Secretary for Energy Efficiency and Renewable Energy, Office of Vehicle Technologies of the U.S. Department of Energy under the Battery Materials Research (BMR) Program and Battery 500 Consortium. D.T.B. and P.E.R. acknowledge support from the National Science Foundation Graduate Research Fellowship Program. SEM was performed at the Stanford Nano Shared Facilities (SNSF), supported by the National Science Foundation under Award ECCS-1542152. NMR was performed at the NMR Facility in the Stanford Department of Chemistry. The authors thank Professor Christopher Chidsey for helpful discussion.

REFERENCES

(1) Chu, S.; Cui, Y.; Liu, N. The Path towards Sustainable Energy. *Nat. Mater.* **2017**, *16* (1), 16–22.

(2) Fang, C.; Wang, X.; Meng, Y. S. Key Issues Hindering a Practical Lithium-Metal Anode. *Trends Chem.* **2019**, *1* (2), 152–158.

(3) Attia, P. M.; Das, S.; Chueh, W. C.; Harris, S. J.; Bazant, M. Z. Electrochemical Kinetics of SEI Growth on Carbon Black: Part I. Experiments. *J. Electrochem. Soc.* **2019**, *166* (4), 97–106.

(4) Zhuo, Z.; Lu, P.; Delacourt, C.; Qiao, R.; Xu, K.; Pan, F.; Harris, S. J.; Yang, W. Breathing and Oscillating Growth of Solid-Electrolyte-Interphase upon Electrochemical Cycling. *Chem. Commun.* **2018**, *54*, 814–817.

(5) Lu, P.; Li, C.; Schneider, E. W.; Harris, S. J. Chemistry, Impedance, and Morphology Evolution in Solid Electrolyte Interphase Films during Formation in Lithium Ion Batteries. *J. Phys. Chem. C* **2014**, *118* (2), 896–903.

(6) Li, Y.; Huang, W.; Li, Y.; Pei, A.; Boyle, D. T.; Cui, Y. Correlating Structure and Function of Battery Interphases at Atomic Resolution Using Cryoelectron Microscopy. *Joule* **2018**, *2* (10), 2167–2177.

(7) Huang, W.; Boyle, D. T.; Li, Y.; Li, Y.; Pei, A.; Chen, H.; Cui, Y. Nanostructural and Electrochemical Evolution of the Solid-Electrolyte Interphase on CuO Nanowires Revealed by Cryogenic Electron Microscopy and Impedance Spectroscopy. *ACS Nano* **2019**, *13* (1), 737–744.

(8) Pei, A.; Zheng, G.; Shi, F.; Li, Y.; Cui, Y. Nanoscale Nucleation and Growth of Electrodeposited Lithium Metal. *Nano Lett.* **2017**, *17* (2), 1132–1139.

(9) Wood, K. N.; Kazyak, E.; Chadwick, A. F.; Chen, K. H.; Zhang, J. G.; Thornton, K.; Dasgupta, N. P. Dendrites and Pits: Untangling the Complex Behavior of Lithium Metal Anodes through Operando Video Microscopy. *ACS Cent. Sci.* **2016**, *2* (11), 790–801.

(10) Ren, X.; Zhang, Y.; Engelhard, M. H.; Li, Q.; Zhang, J. G.; Xu, W. Guided Lithium Metal Deposition and Improved Lithium Coulombic Efficiency through Synergistic Effects of $LiAsF_6$ and Cyclic Carbonate Additives. *ACS Energy Lett.* **2018**, *3* (1), 14–19.

(11) Peled, E.; Menkin, S. Review—SEI: Past, Present and Future. *J. Electrochem. Soc.* **2017**, *164* (7), A1703–A1719.

(12) Baranski, A. S.; Drogowska, M. A.; Fawcett, W. R. The Kinetics of Electroreduction of Li Ions in Tetrahydrofuran at Mercury and Mercury Amalgam Electrodes. *J. Electroanal. Chem. Interfacial Electrochem.* **1986**, *215*, 237–247.

(13) Baranski, A. S.; Fawcett, W. R. Electroreduction of Alkali Metal Cations Part 1. - Effects of Solution Composition. *J. Chem. Soc., Faraday Trans. 1* **1980**, *76*, 1962–1977.

(14) Berliner, M. D.; McGill, B. C.; Majeed, M.; Hallinan, D. T. Electrochemical Kinetics of Lithium Plating and Stripping in Solid Polymer Electrolytes: Pulsed Voltammetry. *J. Electrochem. Soc.* **2019**, *166* (2), A297–A304.

(15) Tao, R.; Bi, X.; Li, S.; Yao, Y.; Wu, F.; Wang, Q.; Zhang, C.; Lu, J. Kinetics Tuning the Electrochemistry of Lithium Dendrites Formation in Lithium Batteries through Electrolytes. *ACS Appl. Mater. Interfaces* **2017**, *9* (8), 7003–7008.

(16) Davidson, R.; Verma, A.; Santos, D.; Hao, F.; Fincher, C.; Xiang, S.; van Buskirk, J.; Xie, K.; Pharr, M.; Mukherjee, P.; Banerjee, S. Formation of Magnesium Dendrites during Electrodeposition. *ACS Energy Lett.* **2019**, *4* (2), 375–376.

(17) Winand, R. Electrodeposition of Metals and Alloys-New Results and Perspectives. *Electrochim. Acta* **1994**, *39* (8/9), 1091–1105.

(18) Hao, F.; Verma, A.; Mukherjee, P. P. Mesoscale Complexations in Lithium Electrodeposition. *ACS Appl. Mater. Interfaces* **2018**, *10* (31), 26320–26327.

(19) Cogswell, D. A. Quantitative Phase-Field Modeling of Dendritic Electrodeposition. *Phys. Rev. E* **2015**, *92* (1), 011301.

(20) Lopez, J.; Pei, A.; Oh, J. Y.; Wang, G. J. N.; Cui, Y.; Bao, Z. Effects of Polymer Coatings on Electrodeposited Lithium Metal. *J. Am. Chem. Soc.* **2018**, *140* (37), 11735–11744.

(21) Shi, F.; Pei, A.; Vailionis, A.; Xie, J.; Liu, B.; Zhao, J.; Gong, Y.; Cui, Y. Strong Texturing of Lithium Metal in Batteries. *Proc. Natl. Acad. Sci. U. S. A.* **2017**, *114* (46), 12138−12143.
(22) Liu, Y.; Lin, D.; Li, Y.; Chen, G.; Pei, A.; Nix, O.; Li, Y.; Cui, Y. Solubility-Mediated Sustained Release Enabling Nitrate Additive in Carbonate Electrolytes for Stable Lithium Metal Anode. *Nat. Commun.* **2018**, *9* (1), 3656.
(23) Kushima, A.; So, K. P.; Su, C.; Bai, P.; Kuriyama, N.; Maebashi, T.; Fujiwara, Y.; Bazant, M. Z.; Li, J. Liquid Cell Transmission Electron Microscopy Observation of Lithium Metal Growth and Dissolution: Root Growth, Dead Lithium and Lithium Flotsams. *Nano Energy* **2017**, *32*, 271−279.
(24) Pletcher, D.; Rohan, J. F.; Ritchie, A. G. Microelectrode studies of the lithium/propylene carbonate system—Part I. Electrode reactions at potentials positive to lithium deposition. *Electrochim. Acta* **1994**, *39* (10), 1369−1376.
(25) Verbrugge, M. W.; Koch, B. J. Microelectrode Study of the Lithium/Propylene Carbonate Interface: Temperature and Concentration Dependence of Physicochemical Parameters. *J. Electrochem. Soc.* **1994**, *141* (11), 3053−3059.
(26) Verbrugge, M. W.; Koch, B. J. Microelectrode Investigation of Ultrahigh-Rate Lithium Deposition and Stripping. *J. Electroanal. Chem.* **1994**, *367* (1−2), 123−129.
(27) Hedges, W. M.; Pletcher, D.; Gosden, C. Microelectrode Studies of the Li/Li^+ Couple in $SOCl_2/LiAlCl_4$. *J. Electrochem. Soc.* **1987**, *134*, 1334−1340.
(28) Genders, J. D.; Hedges, W. M.; Pletcher, D. Application of Microelectrodes to the Study of the Li, Li^+ Couple in Ether Solvents. Part 1. *J. Chem. Soc., Faraday Trans. 1* **1984**, *80*, 3399−3408.
(29) Aurbach, D. *Nonaqueous Electrochemistry*; Dekker, M., Ed.; New York, 1999.
(30) Bard, A. J.; Faulkner, L. R. *Electrochemical Methods Fundamentals and Applications*; John Wiley and Sons, Inc.; New Jersey, 2001.
(31) Wibowo, R.; Jones, S. E. W.; Compton, R. G. Kinetic and Thermodynamic Parameters of the Li/Li^+ Couple in the Room Temperature Ionic Liquid N-Butyl-N-methylpyrrolidinium Bis-(trifluoromethylsulfonyl) Imide in the Temperature Range 298−318 K: A Theoretical and Experimental Study Using Pt and Ni Electrodes. *J. Phys. Chem. B* **2009**, *113*, 12293−12298.
(32) Odziemkowski, M.; Irish, D. E. An Electrochemical Study of the Reactivity at the Lithium Electrolyte/Bare Lithium Metal Interface I. Purified Electrolytes. *J. Electrochem. Soc.* **1992**, *139* (11), 3063−3074.
(33) Hinatsu, J. T.; Foulkes, F. R. Electrochemical Kinetic Parameters for the Cathodic Deposition of Copper from Dilute Aqueous Acid Sulfate Solutions. *Can. J. Chem. Eng.* **1991**, *69*, 571−577.
(34) Reinmuth, W. H. Irreversible Systems in Stationary Electrode Polarography. *Anal. Chem.* **1960**, *32* (13), 1891−1892.
(35) Nicholson, R. S.; Shain, I. Theory of Stationary Electrode Polarography. *Anal. Chem.* **1964**, *36* (4), 706−723.
(36) Marcus, R. A. On the Theory of Electron-Transfer Reactions. VI. Unified Treatment for Homogeneous and Electrode Reactions. *J. Chem. Phys.* **1965**, *43* (2), 679−701.
(37) Hush, N. S. Adiabatic Rate Processes at Electrodes. I. Energy-Charge Relationships. *J. Chem. Phys.* **1958**, *28* (5), 962−972.
(38) Chidsey, C. E. D. Free Energy and Temperature Dependence of Electron Transfer at the Metal-Electrolyte Interface. *Science* **1991**, *251*, 919−922.
(39) Bazant, M. Z. Theory of Chemical Kinetics and Charge Transfer based on Nonequilibrium Thermodynamics. *Acc. Chem. Res.* **2013**, *46* (5), 1144−1160.
(40) Bai, P.; Bazant, M. Z. Charge Transfer Kinetics at the Solid-Solid Interface in Porous Electrodes. *Nat. Commun.* **2014**, *5*, 3585.
(41) Fawcett, W. R. Potential Dependence of the Elementary Steps in the Kinetics of Electrode Reactions Involving Amalgam Formation. *J. Phys. Chem.* **1989**, *93* (6), 2675−2682.
(42) Pinto, L. M. C.; Spohr, E.; Quaino, P.; Santos, E.; Schmickler, W. Why Silver Deposition Is so Fast - or the Enigma of Metal Deposition Unravelled. *Angew. Chem., Int. Ed.* **2013**, *52*, 7883−7885.
(43) Xu, K. Electrolytes and Interphases in Li-ion Batteries and Beyond. *Chem. Rev.* **2014**, *114*, 11503−11618.
(44) Gileadi, E. The Enigma of Metal Deposition. *J. Electroanal. Chem.* **2011**, *660* (2), 247−253.
(45) Liu, Y. P.; Newton, M. D. Reorganization Energy for Electron Transfer at Film-Modified Electrode Surfaces: A Dielectric Continuum Model. *J. Phys. Chem.* **1994**, *98* (29), 7162−7169.
(46) Sankarasubramanian, S.; Seo, J.; Mizuno, F.; Singh, N.; Prakash, J. Elucidating the Oxygen Reduction Reaction Kinetics and the Origins of the Anomalous Tafel Behavior at the Lithium-Oxygen Cell Cathode. *J. Phys. Chem. C* **2017**, *121* (9), 4789−4798.
(47) DeCaluwe, S. C.; Weddle, P. J.; Zhu, H.; Colclasure, A. M.; Bessler, W. G.; Jackson, G. S.; Kee, R. J. On the Fundamental and Practical Aspects of Modeling Complex Electrochemical Kinetics and Transport. *J. Electrochem. Soc.* **2018**, *165* (13), E637−E658.
(48) Li, Y.; Qi, Y. Energy Landscape of the Charge Transfer Reaction at the Complex Li/SEI/Electrolyte Interface. *Energy Environ. Sci.* **2019**, *12*, 1286−1295.
(49) Liu, H.; Zhou, H.; Lee, B.; Xing, X.; Gonzalez, M.; Liu, P. Suppressing Lithium Dendrite Growth with a Single-Component Coating. *ACS Appl. Mater. Interfaces* **2017**, *9*, 30635.
(50) Xu, K. Nonaqueous Liquid Electrolytes for Lithium-Based Rechargeable Batteries. *Chem. Rev.* **2004**, *104*, 4303−4417.
(51) Cahen, Y. M.; Handy, P. R.; Roach, E. T.; Popov, A. I. Spectroscopic Studies of Ionic Solvation. XVI. Lithium-7 and Chlorine-35 Nuclear Magnetic Resonance Studies in Various Solvents. *J. Phys. Chem.* **1975**, *79* (1), 80−85.
(52) Kondo, K.; Sano, M.; Hiwara, A.; Omi, T.; Fujita, M.; Kuwae, A.; Iida, M.; Mogi, K.; Yokoyama, H. Conductivity and Solvation of Li + Ions of $LiPF_6$ in Propylene Carbonate Solutions. *J. Phys. Chem. B* **2000**, *104* (20), 5040−5044.
(53) Jiang, B.; Ponnuchamy, V.; Shen, Y.; Yang, X.; Yuan, K.; Vetere, V.; Mossa, S.; Skarmoutsos, I.; Zhang, Y.; Zheng, J. The Anion Effect on Li^+ Ion Coordination Structure in Ethylene Carbonate Solutions. *J. Phys. Chem. Lett.* **2016**, *7* (18), 3554−3559.
(54) Miao, W.; Ding, Z.; Bard, A. J. Solution Viscosity Effects on the Heterogeneous Electron Transfer Kinetics of Ferrocenemethanol in Dimethyl Sulfoxide-Water Mixtures. *J. Phys. Chem. B* **2002**, *106* (6), 1392−1398.
(55) Zhang, X.; Leddy, J.; Bard, A. J. Dependence of Rate Constants of Heterogeneous Electron Transfer Reactions on Viscosity. *J. Am. Chem. Soc.* **1985**, *107* (12), 3719−3721.
(56) Kwon, K.; Evans, J. W. Viscosity Changes of Li Battery Electrolytes and Their Long-Term Effect on the Frequency of EQCM Electrodes. *Electrochem. Solid-State Lett.* **2002**, *5* (3), A59.
(57) Dougassa, Y. R.; Jacquemin, J.; El Ouatani, L.; Tessier, C.; Anouti, M. Viscosity and Carbon Dioxide Solubility for $LiPF_6$, LiTFSI, and LiFAP in Alkyl Carbonates: Lithium Salt Nature and Concentration Effect. *J. Phys. Chem. B* **2014**, *118* (14), 3973−3980.
(58) Zaban, A.; Zinigrad, E.; Aurbach, D. Impedance Spectroscopy of Lithium Electrodes. 4. A General Simple Model of the Li-Solution Interphase in Polar Aprotic Systems. *J. Phys. Chem.* **1996**, *100*, 3089−3101.
(59) Magnussen, O. M.; Groß, A. Toward an Atomistic-Scale Understanding of Electrochemical Interface Structure and Dynamics. *J. Am. Chem. Soc.* **2019**, *141*, 4777−4790.

https://dx.doi.org/10.1021/acsenergylett.0c00031
ACS Energy Lett. 2020, 5, 701−709